https://doi.org/10.5194/egusphere-2026-3563
Preprint. Discussion started: 8 July 2026
© Author(s) 2026. CC BY 4.0 License.

Persistent and non-negligible aerodynamic entrainment during dust emission: new evidence from field observations and wind tunnel experiments

Shengfei Yang[1,2], Heqiang Du[1], Yawei Fan[1,2], Zongxing Li[1], Yongjie Liu[1,2]

[1]State Key Laboratory of Ecological Safety and Sustainable Development in Arid Lands, Northwest Institute of Eco-Environment and Resources, Chinese Academy of Sciences, Lanzhou, 730000, China

[2]University of Chinese Academy of Sciences, Beijing, 100049, China

Correspondence to: Heqiang Du (duheqiang@lzb.ac.cn)

Abstract. Dust emission is a key process in wind erosion that influences climate and air quality. Consequently, the physical mechanisms of dust emission have attracted widespread attention. However, whether aerodynamic entrainment can persist during natural dust emission events remains debated, and this mechanism is often neglected or treated as secondary in dust emission parameterizations. To address this dispute, we combine field observations and wind tunnel experiments to investigate the persistence and contribution of aerodynamic entrainment. Field observations show that, in the observed plots where saltation rarely occurred, aerodynamic dust entrainment persisted throughout the emission process, whereas in most of the observed plots, the threshold friction velocity for dust entrainment (TFVa) was generally lower than that for saltation initiation. Even where the TFVa exceeded that for saltation, dust emission persisted beyond the cessation of saltation and its emission rate was enhanced by saltation disturbance. Wind tunnel experiments further demonstrated that aerodynamic entrainment persisted and contributed substantially to total dust emissions, accounting for 16−62%. Moreover, the enhancement of dust emission by saltation resulted primarily from surface renewal and aggregate breakdown, which continuously replenished erodible fine particles. Furthermore, existing dust emission models based solely on aerodynamic entrainment or saltation bombardment fail to reproduce observed dust emission magnitude and temporal dynamics. Together, these findings indicate that aerodynamic entrainment is persistent and non-negligible, while saltation contributes not only through dust production but also by modifying surface erodibility. We therefore propose an "entrainment–saltation–renewal–entrainment" framework and suggest future models should consider coupled multi-mechanism processes.

1 Introduction

Dust emission is a critical phase of wind erosion, with the emitted particles constituting a major component of natural atmospheric aerosols (Engelstaedter et al., 2006; Thompson and Ridgwell, 2002; Zhu et al., 2019). These aerosols, in turn, exert significant impacts on climate change, ecological systems, air quality, and human health. This is because they can reduce atmospheric visibility (Engelstaedter et al., 2006); alter the radiative balance of the Earth–atmosphere system through direct,

https://doi.org/10.5194/egusphere-2026-3563
Preprint. Discussion started: 8 July 2026
© Author(s) 2026. CC BY 4.0 License.

semidirect, and indirect radiative effects (Hansen et al., 1997; Huang et al., 2006; Koren et al., 2004; Li et al., 2018; Liao and Seinfeld, 1998; Sokolik and Toon, 1999); and transport elements such as iron and nitrogen to marine ecosystems via long-range atmospheric transport (Ravi et al., 2011; Ridgwell and Watson, 2002). Furthermore, the inhalation of dust aerosols into human lungs can trigger cardiovascular and respiratory diseases, posing significant threats to human health (Liu et al., 2016). As the initial process of dust loading in the atmosphere, the physical mechanism of dust emission has been investigated by scholars (Anderson and Haff, 1988; Bagnold, 1941; Du et al., 2024; Kjelgaard et al., 2004; Kok et al., 2012; Loosmore and Hunt, 2000; Shao et al., 1993; Sweeney and Mason, 2013; Zhang et al., 2016).

Three mechanisms of dust emission in wind erosion events are commonly identified: (1) direct aerodynamic entrainment, (2) saltation bombardment, and (3) soil aggregate disintegration (Kok et al., 2012; Shao, 2008; Újvári et al., 2016). In traditional dust emission theory and in many commonly used parameterizations, direct aerodynamic entrainment has often been regarded as difficult to sustain and is therefore commonly treated as intermittent, or neglected relative to saltation-bombardment-driven emission (Kok et al., 2012; Shao, 2001, 2008; Zender et al., 2003). This consensus is primarily based on two traditional viewpoints: (1) strong cohesive forces due to van der Waals interactions exist between fine particles, which significantly increase the threshold friction velocity required for their entrainment; and (2) free dust availability at the surface has often been assumed to be constrained by source limitation, which may restrict the persistence of direct aerodynamic entrainment (Macpherson et al., 2008; Shao, 2008; Újvári et al., 2016 Greeley and Iversen, 1985；Shao et al.,1993；Marticorena et al., 1997). Consequently, numerous dust emission models based on saltation bombardment have been developed and applied to regional and global dust simulations (Marticorena and Bergametti, 1995; Zakey et al., 2006; Zender et al., 2003). However, significant discrepancies exist between a substantial body of simulation results and field-observed dust fluxes (Haustein et al., 2015; Zhao et al., 2020). These discrepancies arise in part from a lack of understanding of the physical mechanism of dust emission; to be precise, these models, which are based on saltation bombardment mechanisms, cannot adequately depict the complexity of dust emission processes.

In recent years, emerging observational and theoretical evidence has challenged this classic paradigm. Field and wind-tunnel studies have shown that aerodynamic entrainment can generate substantial dust fluxes (Du et al., 2024; Sweeney and Mason, 2013). And, the concept of surface renewal, proposing that wind erosion can continuously expose underlying fine particles by stripping away surface coarse particles, suggests that dust supply limitations might be a pseudo-issue in continuous wind erosion events (Shao et al., 2025; Zhang et al., 2016). Additionally, other studies have further demonstrated that dust emission can occur intermittently in the absence of saltation, because turbulent large eddies may temporarily produce sufficiently strong surface shear stress to entrain fine particles (Klose et al., 2014; Klose and Shao, 2012; Zhang et al., 2022). Therefore, these findings have prompted the aeolian physics community to reconsider the role and contribution of aerodynamic

https://doi.org/10.5194/egusphere-2026-3563
Preprint. Discussion started: 8 July 2026
© Author(s) 2026. CC BY 4.0 License.

entrainment to dust emission. To date, the study of the physical mechanisms of dust emission in wind erosion events still has three major issues: (1) whether aerodynamic entrainment can persist, (2) the extent of its contribution to dust emission, and (3) what role saltation bombardment plays in the emission process. To address these issues, we combined field observations with wind-tunnel experiments to investigate dust emission processes under natural and controlled conditions, with particular emphasis on aerodynamic entrainment and saltation disturbance.

2 Materials and methods

2.1 Field observations

2.1.1 Field observation methods and measured variables

To investigate the mechanisms of dust emission in wind erosion events under natural conditions, short-term wind erosion observations were conducted via a wind erosion observation system in the desert steppe of central Inner Mongolia and the Mu Us sandy farmland, both in northern China. The wind erosion observation system integrates a multiparameter synchronous monitoring setup comprising ultrasonic anemometers, Sensit wind erosion flux sensors (H14-LIN), and DustTrak aerosol monitors (Figure 1a). Four ultrasonic anemometers were installed at heights of 0.05, 0.2, 1 and 2 m to continuously record wind speed at 15-s intervals. Near-surface wind erosion dynamics were monitored using Sensit sensors, which simultaneously captured the particle impact energy and frequency at heights of 0.05 m and 0.2 m, with a sampling frequency of 15 seconds. All time-series data were stored locally via a CR300 series data logger. The aerosol concentration was monitored using two DustTrak aerosol monitors, with the sampling ports installed at heights of 1 m and 2 m, to simultaneously collect the PM_{10} mass concentration data. To minimize the influence of horizontal dust advection, the instrument array was deployed along the prevailing local wind direction during each observation period, so that the inferred flux primarily reflected local dust emission rather than advected dust from upwind sources, although advection cannot be completely ruled out under field conditions.

The observations were conducted in April and May 2022 across 27 plots in arid and semiarid regions, representing four typical soil types: loamy sand, sandy loam, loam, and silt (Figure 1b). Plots in the Mu Us sandy farmland were established on largely bare surfaces with no obvious vegetation or residue cover (Figure 1a), whereas plots in the desert steppe of central Inner Mongolia were located in areas with sparse vegetation cover (Figure S1). The land-use types of all plots are summarized in Table S1, and each plot was monitored for 3~6 h.

https://doi.org/10.5194/egusphere-2026-3563
Preprint. Discussion started: 8 July 2026
© Author(s) 2026. CC BY 4.0 License.

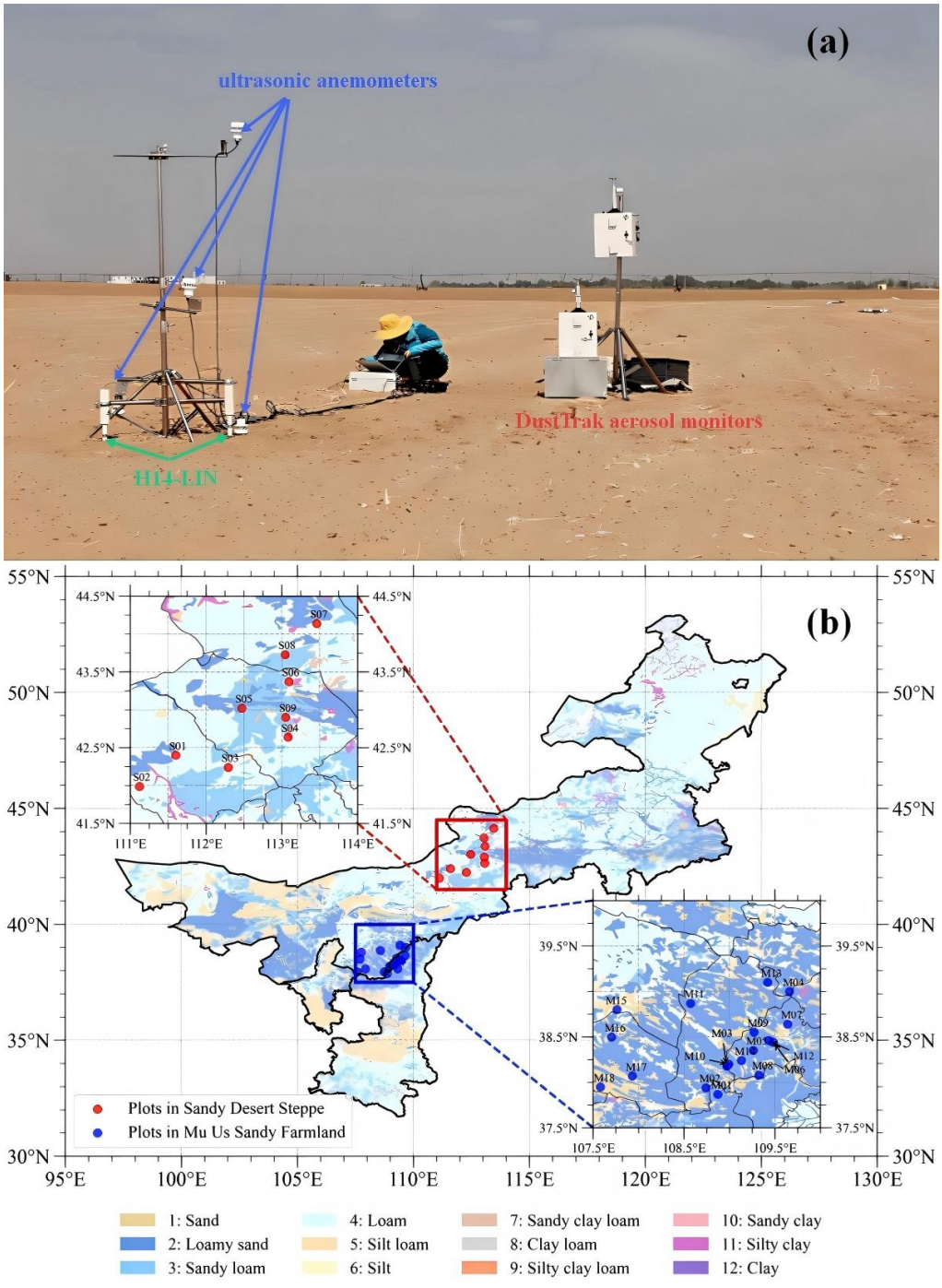

Figure 1. (a) A wind erosion observation system; (b) distribution of field observation plots; color-filled areas represent soil texture.

2.1.2 Calculation of PM_{10} emission flux and threshold friction velocity

Following previous studies, the vertical emission flux of PM_{10} (F) was calculated using PM_{10} concentrations at two

https://doi.org/10.5194/egusphere-2026-3563
Preprint. Discussion started: 8 July 2026
© Author(s) 2026. CC BY 4.0 License.

different heights. The calculation formula is as follows:

$$F = \frac{ku_* (c_1 - c_2)}{\ln(z_2/z_1)} \quad (1)$$

where k=0.4 is the von Kármán constant; c_1 and c_2 are the PM_{10} concentrations at heights z_1 and z_2, respectively; and u^*(m/s) is the friction velocity, which is calculated via Equation (2):

$$u_z = \frac{u_*}{k} \ln(z/z_0) \quad (2)$$

where u_z (m/s) is the wind speed at height z and where z_0 (m) is the aerodynamic roughness length.

This calculation method is based on the assumption of neutral or near-neutral atmospheric conditions(Dupont, 2022; Kjelgaard et al., 2004; Sharratt et al., 2007; Wagner et al., 2021). To evaluate the validity of this assumption, high-resolution wind speed measurements at 0.05, 0.2, 1, and 2 m above the surface at each observation plot were used to fit logarithmic wind profiles at hourly resolution. Across all 27 field plots, the mean coefficient of determination (R^2) for the log-law fits was 0.92 (range: 0.84~0.97), with the vast majority exceeding 0.90 (Table S1), indicating that the observed wind profiles are generally well described by the logarithmic wind law. Therefore, the use of a neutral wind profile approximation as a first-order estimate of PM_{10} emission flux is justified in this study.

The z_0 values for all plots were derived by fitting the logarithmic wind profile between wind speed $u(z)$ and measurement height z, and were summarized in Table S1. The corresponding u_* for each plot was then obtained simultaneously from the same logarithmic wind-profile fitting. To minimize observational noise, the two DustTrak instruments were rigorously inter-calibrated at the same sampling height before each observation. Measurements below 0.001 mg·m^{-3}, which corresponds to the instrumental resolution, were considered noise and were excluded from subsequent analysis.

In each plot, the data points where saltation occurred (saltation number tested by Sensit sensors > 0) were selected, and the minimum value of the synchronous wind speed was taken as the threshold wind speed of saltation initiation. The threshold friction velocity of saltating sand particles (TFVs) was then calculated via Equation (2). Additionally, data points where dust emission occurred without accompanying saltation bombardment were selected, and the synchronous emissions were attributed to aerodynamic entrainment. The TFV for PM_{10} entrainment (TFVa) in each plot was subsequently calculated via the TFV calculation method.

Shao and Klose (2016) pointed out that interparticle cohesive forces and the associated initiation process are inherently stochastic. Therefore, especially for the aerodynamic entrainment of fine particles, threshold friction velocity should not be interpreted as a single deterministic value, but rather as an event-based indicator associated with the probability of initiation. In this context, the TFV_a and TFV_s derived in this study were not intended to define intrinsic deterministic thresholds for dust or saltating particles. Instead, under the given observation period, sampling frequency, and instrument detection conditions,

https://doi.org/10.5194/egusphere-2026-3563
Preprint. Discussion started: 8 July 2026
© Author(s) 2026. CC BY 4.0 License.

they represent the minimum observed friction velocities associated with the onset of PM_{10} emission and detected saltation, that is, apparent left-tail values of the observed TFV distributions. Accordingly, they were used to compare the wind conditions associated with the onset of PM_{10} emission and saltation, and to assess whether dust emission could occur in the absence of detected saltation bombardment.

2.1.3 Soil sample collection and testing

During the observation period, surface soil samples were simultaneously collected from each plot (sampling specifications: 10 × 10 cm quadrat, sampling depth of 5 cm, with three replicates per plot). After being sealed in airtight bags for preservation, the soil samples were tested for their particle size distribution (PSD) using a Malvern Mastersize-3000 (Malvern Instruments Ltd., Malvern, UK) in the laboratory. In accordance with the soil sample testing method proposed by Shao (2008), two types of preprocessing—nondispersive (without chemical dispersants) and dispersive (with chemical dispersants)—were carried out before being tested with the Mastersize-3000. The PSD test results with the former preprocessing were referred to as soil particle size distributions under minimal disturbance conditions (PCMDS), and those with the latter preprocessing were referred to as soil particle size distributions under fully disturbed conditions (PCFDS) (Shao, 2008). On the basis of these results, we calculated the mass fractions of PM_{10} and saltation-sized particles (50~300 μm) under both treatment conditions. Spearman's rank correlation analysis was subsequently performed to evaluate the relationships between the following variables: (1) the correlation between the TFV and PM_{10} content in the PCMDS and PCFDS and (2) the correlation between the TFVa and the mass fraction of saltation-sized particles in the PCMDS and PCFDS.

2.2 Wind tunnel experiments

2.2.1 Experimental setup

To further investigate the dust emission forms and the role of saltation bombardment in wind erosion events, wind tunnel experiments were carried out at the Gansu Desert Control Research Institute. The wind tunnel has a total length of 38.9 m and consists of an intake section, a power section, a rectification section, a contraction section, a test section, an adjustable test section, and a diffusion section. The core test section is 16 m long with cross-sectional dimensions of 1.2 × 1.2 m (Figure 2), allowing precise control of wind speeds ranging from 4 to 35 m/s. The experimental conditions were validated by calculating the Froude number ($F_r = U^2/gH$). This parameter fell within the range of 5.4 to 19.1, indicating that the system met the similarity requirements for wind–sand movement. A multiparameter synchronous monitoring system was employed in the experiments: (1) Wind speed profiles were measured using a KIMO pitot tube array. On the basis of the Bernoulli principle, the wind speed at specific heights was calculated from the total static pressure difference across nine vertical heights (0.01,

https://doi.org/10.5194/egusphere-2026-3563
Preprint. Discussion started: 8 July 2026
© Author(s) 2026. CC BY 4.0 License.

0.03, 0.05, 0.08, 0.13, 0.2, 0.3, 0.4, and 0.6 m), with a sampling frequency of 0.5 s. (2) The kinetic energy characteristics of saltating sand particles were measured using Sensit wind erosion sensors installed at heights of 0.05 and 0.10 m. The piezoelectric metal rings in the sensors converted the impact energy of the sand particles into electrical pulse signals, which were recorded digitally at 15-second intervals. (3) Horizontal sand emission flux was obtained via SandFlow4 sand flow sensors installed at heights of 0.10, 0.20, 0.30, and 0.40 m. These sensors, which are based on the principle of acoustic pressure fluctuations, can detect sand flux intensity in a range from 0 to 250 $g \cdot m^{-2} \cdot s^{-1}$ in real time, with a sampling interval of 15 s. (4) The aerosol concentration was monitored using DustTrak aerosol monitors installed at heights of 0.70 and 1.10 m, which continuously measured the mass concentrations of PM_1, $PM_{2.5}$, PM_4, PM_{10}, and PM_{15} through light scattering. The measurement range was 0.001 to 100 $mg \cdot m^{-3}$, with a sampling frequency of 5 s. Photographs of the corresponding instruments are provided in Figure S2.

The experimental soil samples were collected from the surface layer (0–20 cm) of the sandy desert steppe (SDS) in central Inner Mongolia and composited into a single sample. This site was selected for two reasons. First, our previous field observations were conducted in the same desert-steppe environment, enabling direct comparison between field measurements and controlled wind tunnel experiments. Second, SDS soils are characterized by a heterogeneous particle-size distribution that includes both fine particles and abundant coarse grains and aggregates capable of saltation. Such a composition favors intense particle–surface interactions and saltation-induced disturbances, making it particularly suitable for investigating the mechanisms of dust emission and the influence of saltation under controlled conditions. Sampling was conducted only on surface patches with no obvious vegetation or residue cover. The composite soil sample was classified according to the USDA (United States Department of Agriculture) soil texture classification standard (Table 1). The experimental design consisted of groups designated as SDS-*x*-*y*-*z*, where SDS represents the provenance of the soil sample; *x* indicates the presence or absence of an external sand supply in the upwind area of the soil sample to detect the role of external saltation bombardment; *y* denotes the wind speed; and *z* specifies the particle size range of the external saltation sand (Table 2). The collected SDS soil was used as the substrate and was uniformly spread across the sand bed in the wind tunnel testing section (Figure 2). Prior to the main experiment, preliminary tests with progressively increasing wind speed showed that steady dust emission commenced at 8 m/s. On this basis, wind speeds of 8, 10 and 12 m/s were adopted in the main experiment to represent different intensities of dust emission. Additionally, external saltation sand particles were collected from the Mu Us sandy farmland. After being washed to remove dust impurities and air-dried, the samples were sieved into three uniform size fractions: 125~200, 200~300, and 300~450 μm, which served as the external saltation sand source. For the conditions with external saltation sand supply (*x* = "P", presence of external saltation sand), all combinations of the three wind speeds (*y* = 8, 10, and 12 m/s) and the three sand size classes (*z*) were tested; for the conditions without external sand supply (*x* = "A", absence of external saltation sand),

https://doi.org/10.5194/egusphere-2026-3563
Preprint. Discussion started: 8 July 2026
© Author(s) 2026. CC BY 4.0 License.

experiments were conducted at each of the same three wind speeds only, with no z distinction. This yielded a total of 12 experiments (Table 2). To ensure reliability of the results, each experiment was repeated three times.

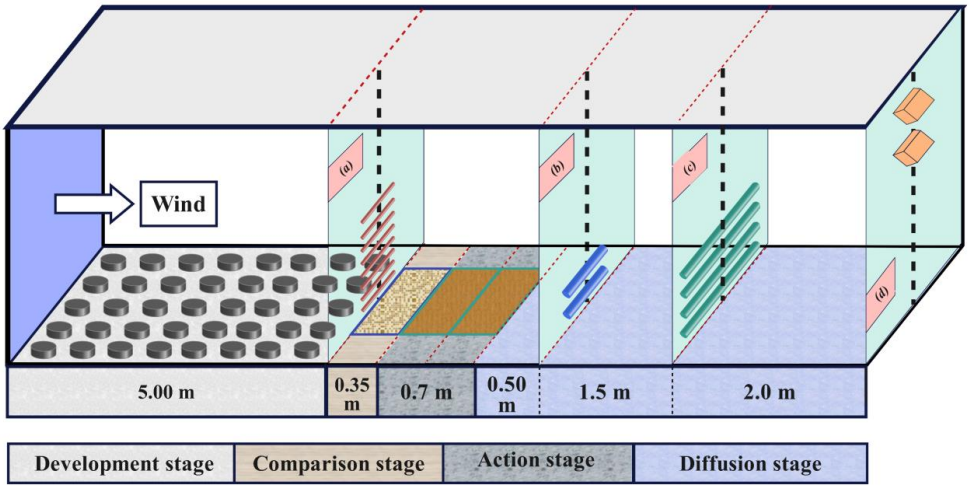

Figure 2. Wind tunnel setup. Panels a–d show the cross-sectional arrangement of the KIMO Pitot tubes, Sensit wind-erosion sensors, SandFlow4 sand-flow sensors and DustTrak aerosol monitors, respectively.

Table 1. Sampling locations and soil property for the wind tunnel experiment samples.

Parameter	Value
Lon (N°)	113.05
Lat (E°)	42.90
Clay (%)	1.54
Silt (%)	11.70
Sand (%)	86.76
Soil Texture	Sand

Table 2. Configuration of the wind tunnel experiments.

Experiment name	Soil sample provenance	Presence (P) or Absence (A) of external sand	Near-surface wind velocity (m/s)	Particle size of external sand (μm)
SDS-A-08-N/A	SDS	A	8	N/A
SDS-A-10-N/A			10	
SDS-A-12-N/A			12	
SDS-P-08-125~200		P	8	125~200
SDS-P-08-200~300				200~300
SDS-P-08-300~450				300~450
SDS-P-10-125~200			10	125~200
SDS-P-10-200~300				200~300
SDS-P-10-300~450				300~450
SDS-P-12-125~200			12	125~200
SDS-P-12-200~300				200~300
SDS-P-12-300~450				300~450

https://doi.org/10.5194/egusphere-2026-3563
Preprint. Discussion started: 8 July 2026
© Author(s) 2026. CC BY 4.0 License.

2.2.2 Calculation of PM_{10} emissions

(1) *F*: measured PM_{10} dust emission flux

185 *F* was calculated using the same method as that applied to the field observations.

(2) $F_{a\text{-}LH00}$: theoretical PM_{10} emission flux from direct aerodynamic entrainment

$F_{a\text{-}LH00}$ was calculated via Equation (3) of the empirical model LH00 proposed by Loosmore and Hunt (2000):

$$F_{a-LH00} = 0.87 \cdot \left(3.6u_*^3\right) \tag{3}$$

where 0.87 represents the PM_{10} mass fraction in emitted dust (Zender et al., 2003), and u_* (m/s) is the friction velocity. Based
190 on the measured wind profiles, the u_* corresponding to constant free-stream wind speeds of 8, 10, and 12 m/s were calculated as 0.71, 0.89, and 1.06, respectively.

(3) $F_{s\text{-}Zender03}$: theoretical PM_{10} emission flux from bulk sandblasting

Rooted in the parameterization of Marticorena and Bergametti (1995), the Zender03 model (Zender et al., 2003) was typically classified as a semi-empirical model (Shao and Dong, 2006). Rather than explicitly resolving the micro-mechanical
195 energetics of saltation bombardment and aggregate disaggregation, this model macroscopically lumps the complex impact processes into a bulk sandblasting mass efficiency (α), which is parameterized empirically based on soil clay content. Following Zender et al. (2003), $F_{s\text{-}Zender03}$ was calculated via Equation (4):

$$F_{s-Zender03} = 0.87\alpha QT \tag{4}$$

where Q represents the total horizontal saltation flux; T=7.0×10^{-4} represents the dust emission correction factor; the coefficient
200 0.87 represents the PM_{10} mass fraction in saltation-induced dust emissions (Zender et al., 2003); and α (m^{-1}) represents the saltation mass efficiency, which quantifies the ability of saltation to effectively emit dust. The α can be calculated via Equation (5):

$$\alpha = 100e^{[(13.4M_{clay} - 6.0)\ln 10]} \tag{5}$$

where M_{clay} is the mass fraction of clay in the soil (Table 1).

205 The Q was derived from the vertical profile of horizontal saltation flux, ($q(z)$). According to Shao and Raupach (1992), $q(z)$ follows an exponential decay law, as expressed in Equation (6). The horizontal flux of saltating sand particles, q, was measured at four heights via the SandFlow4 sand flux sensor, and the $q(z)$ profile was obtained via nonlinear regression fitting.

$$q(z) = ce^{az^2 + bz} \tag{6}$$

The Q was then calculated via Equation (7), integrating over the characteristic height range of saltation motion (0~0.4 m).

210 $$Q = \int_0^{0.4} q(z)\,dz \tag{7}$$

https://doi.org/10.5194/egusphere-2026-3563
Preprint. Discussion started: 8 July 2026
© Author(s) 2026. CC BY 4.0 License.

3 Results

3.1 Evidence for the persistent occurrence of dust direct aerodynamic entrainment

For each observation plot, the recorded data at any given moment can be categorized into the following four scenarios: (I) both saltation bombardment and PM_{10} emission occurred, (II) only PM_{10} emission occurred without saltation bombardment that means the PM_{10} emissions resulted from direct aerodynamic entrainment rather than saltation bombardment, (III) saltation bombardment occurred without PM_{10} emission, and (IV) neither saltation bombardment nor PM_{10} emission was observed (i.e., no recorded data). A detailed classification of the 27 field plots is provided in Table S1. A statistical analysis revealed that among all the plots, PM_{10} emissions were observed in 24 plots, saltation was recorded in 23 plots, and data were unavailable for 3 plots.

From the 27 plots, those predominantly exhibiting scenario II were selected. For the eight plots meeting the criteria, time series of F and the synchronous saltation counts were plotted (Figure 3). The results revealed that all the selected plots presented continuous PM_{10} emissions, and at some time points, the instantaneous PM_{10} flux reached 30 $\mu g \cdot m^{-2} \cdot s^{-1}$. These results indicate that continuous dust emission can occur under conditions in which little or no saltation was detected by the Sensit sensors, suggesting that direct aerodynamic entrainment can persist in natural environments and may make an important contribution to dust emission under such conditions.

Although the Sensit sensors may not capture all saltating particles, particularly under weak or intermittent saltation conditions, no field instrument achieves perfect detection efficiency. In the present study, however, each field observation lasted 3–6 h, such that occasional missed detections of saltating particles would have only a very limited influence on the overall interpretation of the results. The absence of detected saltation during most dust emission periods therefore suggests that dust emission can persist in the absence of sustained saltation impacts, indicating that direct aerodynamic entrainment can maintain dust emission under such conditions.

The TFVa and TFVs of each plot are shown in Figure 4. The TFVa ranged between 0.139 and 0.466 m/s, and the TFVs had a wider range from 0.139 to 0.755 m/s. At the plots where both saltation bombardment and aerodynamic entrainment occurred, the TFVa was generally lower than the TFVs (Figure 4 and Figure S3). This result suggests that dust emission does not necessarily require persistent saltation bombardment, and also indicates that dust emission can be initiated under weaker wind conditions than those required for sustained saltation and that direct aerodynamic entrainment is therefore more readily triggered. Accordingly, direct aerodynamic entrainment may contribute significantly to dust emission, particularly under relatively low-wind or weak-saltation conditions.

Statistical analyses revealed that TFVa and TFVs were negatively correlated with their corresponding particle contents (Figure 4). Specifically, the correlation coefficients between TFVa and the PM_{10} content in PCMDS and PCFDS were -0.37

https://doi.org/10.5194/egusphere-2026-3563
Preprint. Discussion started: 8 July 2026
© Author(s) 2026. CC BY 4.0 License.

and -0.31, respectively, neither of which passed the significance test at the 0.05 level. This lack of significant correlation is broadly consistent with classical aeolian physics (Kok et al., 2012; Shao, 2008), suggesting that the notion of "limited dust supply" is not valid. In contrast, the correlation coefficients between the TFVs and saltation particle content in the PCMDS and PCFDS were -0.69 and -0.71, respectively, indicating strong correlations and statistical significance. This finding suggests that the saltation process is more dependent on the content of saltation particles in parent soils.

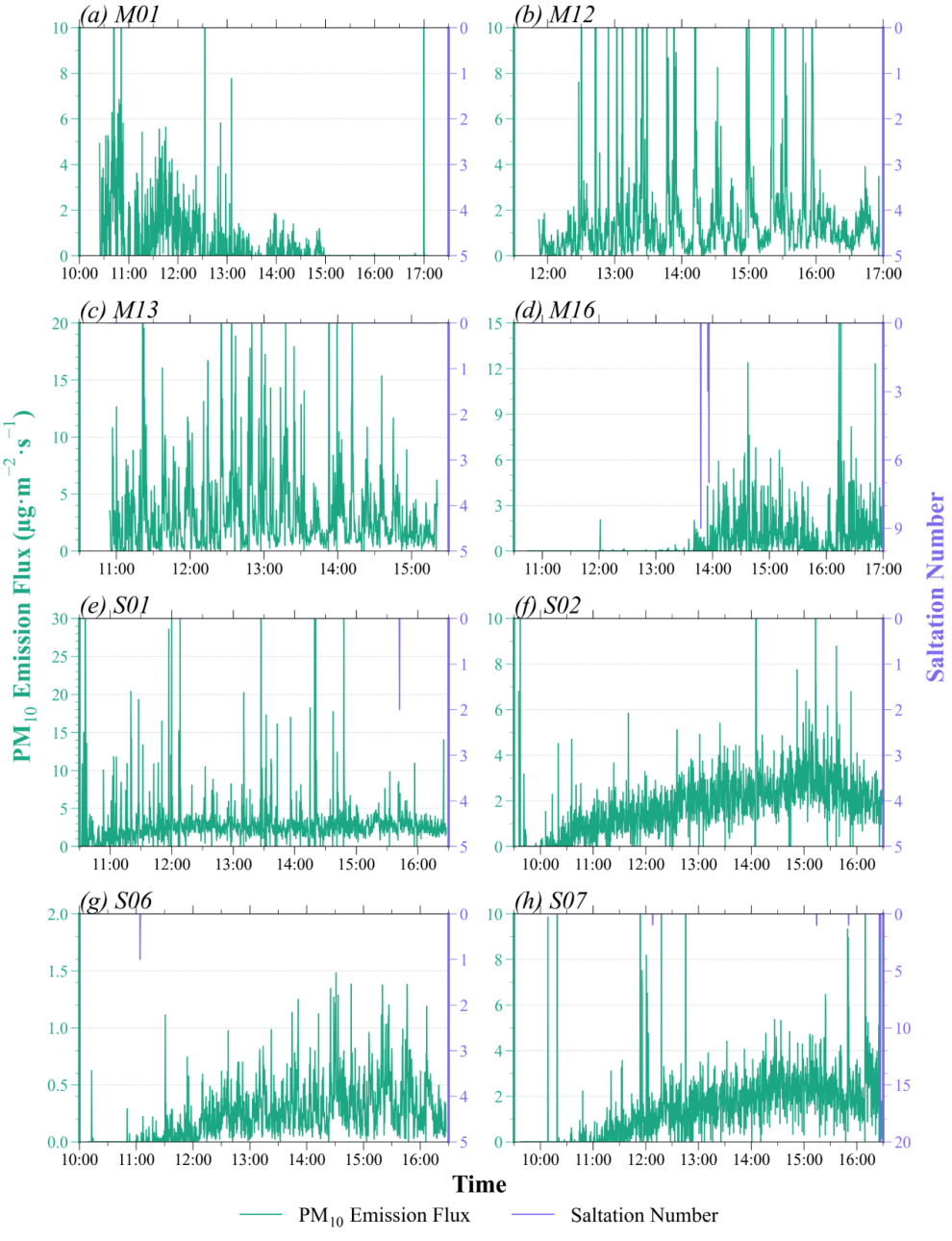

Figure 3. Temporal variation in the PM_{10} emission flux and synchronous saltating particle count.

https://doi.org/10.5194/egusphere-2026-3563
Preprint. Discussion started: 8 July 2026
© Author(s) 2026. CC BY 4.0 License.

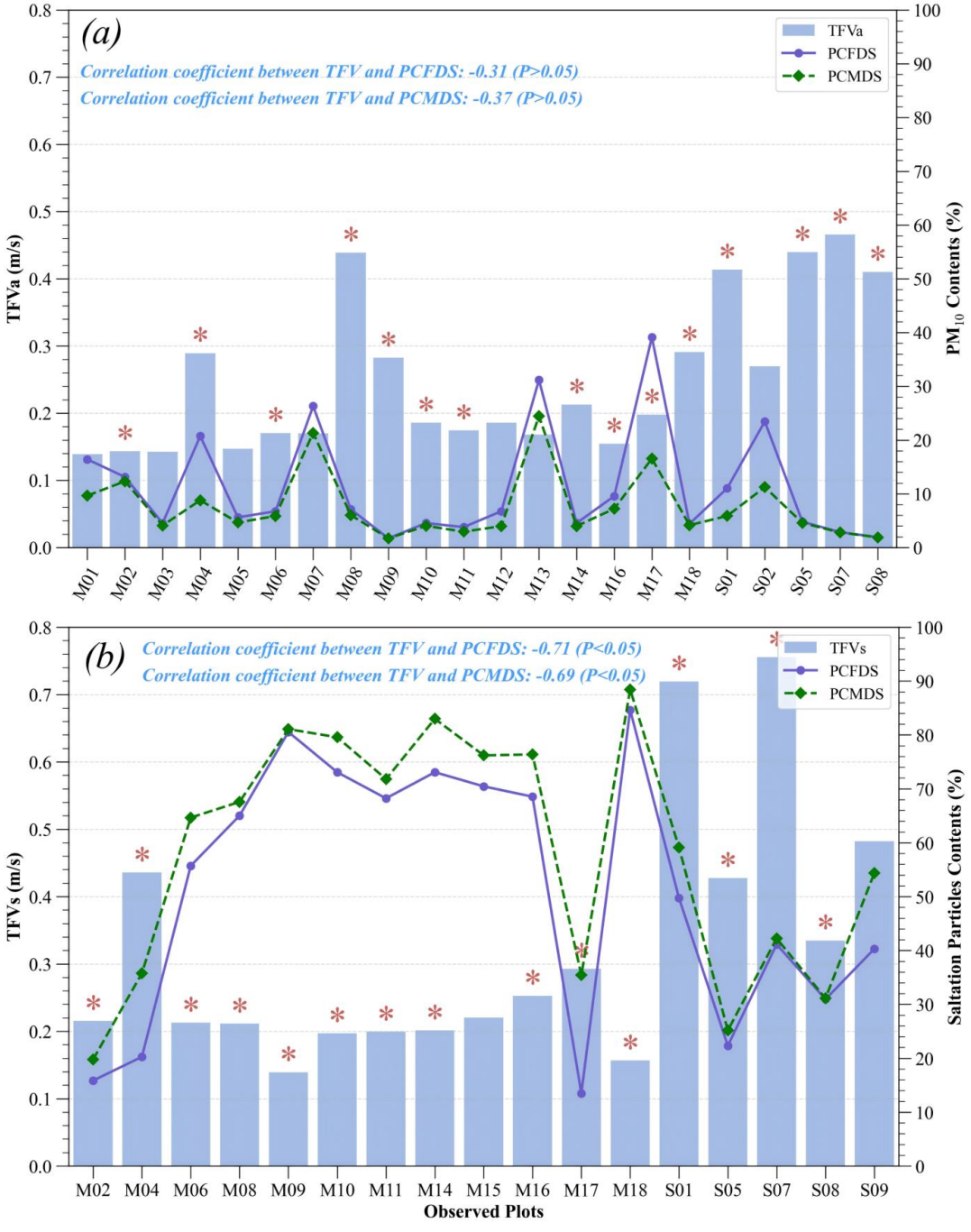

Figure 4. The TFVa, TFVs and soil content for particles in different plots and their correlations with the PCFDS and PCFMS. (a) PM_{10} and (b) saltating sand particles. Note: The red asterisk "*" indicates plots where both saltation bombardment and aerodynamic entrainment were observed.

https://doi.org/10.5194/egusphere-2026-3563
Preprint. Discussion started: 8 July 2026
© Author(s) 2026. CC BY 4.0 License.

3.2 Large fractions of entrained dust are independent of saltation bombardment

As shown in Figure S3, in the plots where both saltation and PM_{10} emissions occurred (M08, M09, M14, M18, S05, and S08), the TFVa was consistently higher than the TFVs. Theoretically, this indicates that wind conditions sufficient to trigger aerodynamic entrainment are also sufficient to induce saltation. As a result, distinguishing whether the emitted PM_{10} was derived by saltation bombardment or aerodynamic entrainment was challenging.

By analyzing the time series of F and the synchronous saltating particle counts at these plots (Figure S4), two emission patterns were observed. The total series in Plots S05, S08, M08, and M18, as well as the latter half series in M14, exhibited intermittent bursts of PM_{10} emission, whereas the total series in M09 and the first half series in M14 showed continuous emission. In all the cases, there were periods where F displayed significant synchronous pulsing with the saltating sand. In these plots, in addition to the synchronous occurrence of PM_{10} emission and saltation, two unique PM_{10} emission patterns were observed: (1) PM_{10} emission occurred in the absence of any recorded saltating sand, referred to as Type A; and (2) a lagged emission phenomenon occurred, where saltating sand ceased for one observation cycle, yet PM_{10} emission continued, referred to as Type B.

On the basis of the above analysis, we counted the total number of dust emission events across the six plots during the observation period, and further calculated the occurrence number, frequency, and maximum F values of Type A and Type B events (Table 3). Type A and B emissions were both observed in all plots, but their occurrence frequencies and emission intensities varied significantly. In Plot M09, PM_{10} displayed continuous emission, and it had the highest number and frequency of Type A emissions (373, 29.58%), with a maximum F of 53.01 $\mu g \cdot m^{-2} \cdot s^{-1}$. This indicates the presence of a direct aerodynamic entrainment process in the plot. During the remaining 70.42% of the observed periods, saltation bombardment and dust emission were concurrently observed, suggesting that sustained saltation may be dynamically synchronized with direct aerodynamic entrainment. This phenomenon may be attributed to surface renewal processes that expose underlying fine particles, enabling a certain amount of dust emission via direct aerodynamic entrainment even in the absence of saltation. Notably, in Plot S08, with intermittently pulsed dust emission, Type A emission accounted for 99.04% of the events, and its maximum F (138.62 $\mu g \cdot m^{-2} \cdot s^{-1}$) was the highest among all the plots. This further and unequivocally verifies that direct aerodynamic entrainment can occur independently of concurrent saltation and is capable of generating persistent dust emission of extremely high intensity. Although Type B emissions were less common overall (0.96% ~ 16.00%), the maximum F values in Plots M09 and M14 (53.01 and 9.56 $\mu g \cdot m^{-2} \cdot s^{-1}$, respectively) were comparable to those of Type A emissions. This indicates that while lagged emissions are relatively rare, they can still contribute significantly to dust flux under certain conditions. In addition, this lagged response suggests that saltation may indirectly trigger subsequent high-intensity dust emission from aerodynamic entrainment. Furthermore, all six plots presented a high frequency of Type A emissions, which reflects a relatively

https://doi.org/10.5194/egusphere-2026-3563
Preprint. Discussion started: 8 July 2026
© Author(s) 2026. CC BY 4.0 License.

high occurrence of direct aerodynamic entrainment under natural conditions.

In summary, direct aerodynamic entrainment exists and can occur continuously. There may be synchronized direct aerodynamic entrainment processes during sustained saltation. The latter may have a significant enhancement effect on the former. To further investigate the role of saltation in dust emissions, wind tunnel experiments were carried out in this study.

Table 3. Statistics of the number, frequency and maximum emission for Type A and B.

Plots	Number			Frequency (%)		Maximum F (μg·m^{-2}·s^{-1})	
	Dust emission events	A	B	A	B	A	B
M08	12	10	1	83.33	8.33	20.07	2.28
M09	1261	373	93	29.58	7.38	53.01	53.01
M14	649	557	23	85.82	3.54	34.17	9.56
M18	117	67	10	57.26	8.55	2.74	2.74
S05	100	73	16	73.00	16.00	16.62	1.09
S08	312	309	3	99.04	0.96	138.62	0.41

3.3 Dust emission mechanism in wind tunnel

To further study the dust emission mechanism, a series of wind tunnel experiments were carried out in which the dust emission processes and magnitudes were compared under two groups of experiments: with external saltation disturbances and without external saltation disturbances. For each set of experiments, we calculated the mean values of F, $F_{a\text{-}LH00}$, $F_{s\text{-}zender03}$, and Q from triplicate measurements, yielding time series of the average measured PM_{10} emission flux, theoretical PM_{10} emission fluxes, and horizontal saltation flux. Specifically, Figures 5 displayed the average time series of F, $F_{a\text{-}LH00}$, and $F_{s\text{-}zender03}$ for the SDS-*x*-*y*-*z* experiments, whereas Figures 6 presented the corresponding average Q time series.

The contribution of aerodynamic entrainment and the corresponding mechanical disturbance were quantified by calculating both the cumulative PM_{10} emission and the cumulative horizontal saltation mass for each experiment. To ensure strict comparability across treatments within the experimental group, the integration cutoff time was unified to the shortest sequence duration, guaranteeing that all cumulative masses—for both PM_{10} emission and saltation transport—were derived over exactly the same time window. The cumulative PM_{10} emissions and the horizontal saltation mass under varying wind speeds and sand supply conditions are presented in Figure 7 and Figure 8, respectively.

3.3.1 Evidence for synchronous aerodynamic entrainment and saltation bombardment

In the SDS-A-8-N/A experiment, the measured Q persistently remained close to zero (Figure 6a). Under classic saltation-driven theory, dust emission under such conditions should be negligible. However, our wind tunnel measurements revealed that the F remained continuous and highly significant throughout the entire 375 s experimental period, sustaining a substantial average magnitude of 0.015 mg·m^{-2}·s^{-1} (Figure 5a). For saltation bombardment was nearly absent in this experiment, this

https://doi.org/10.5194/egusphere-2026-3563
Preprint. Discussion started: 8 July 2026
© Author(s) 2026. CC BY 4.0 License.

persistent *F* was primarily driven by direct aerodynamic entrainment. This empirical evidence unequivocally confirms our field observations: direct aerodynamic entrainment can occur independently and maintain continuous, substantial dust emission.

According to Loosmore and Hunt (2000), the dust emission flux driven by aerodynamic entrainment scales with the cube of wind velocity. Although the empirical proportionality coefficient may involve some uncertainty, the strongly non-linear increase of emission with wind speed is physically robust. As noted earlier, the persistent dust emission in the SDS-A-8-N/A experiment originated entirely from aerodynamic entrainment. Therefore, in all sub-experiments at wind speeds of 10 and 12 m/s (Figure 5), as well as the sand-supplied sub-experiments at 8 m/s, aerodynamic entrainment also occurred continuously. Meanwhile, Figure 6 shows that all SDS-x-10-z and SDS-x-12-z sub-experiments exhibited substantial saltation bombardment, and the SDS-P-8-z sub-experiments generated small but continuous *Q*, indicating that their total emission rates also included a contribution from saltation bombardment. This confirms that aerodynamic entrainment and saltation bombardment are concurrent physical processes during real dust emission.

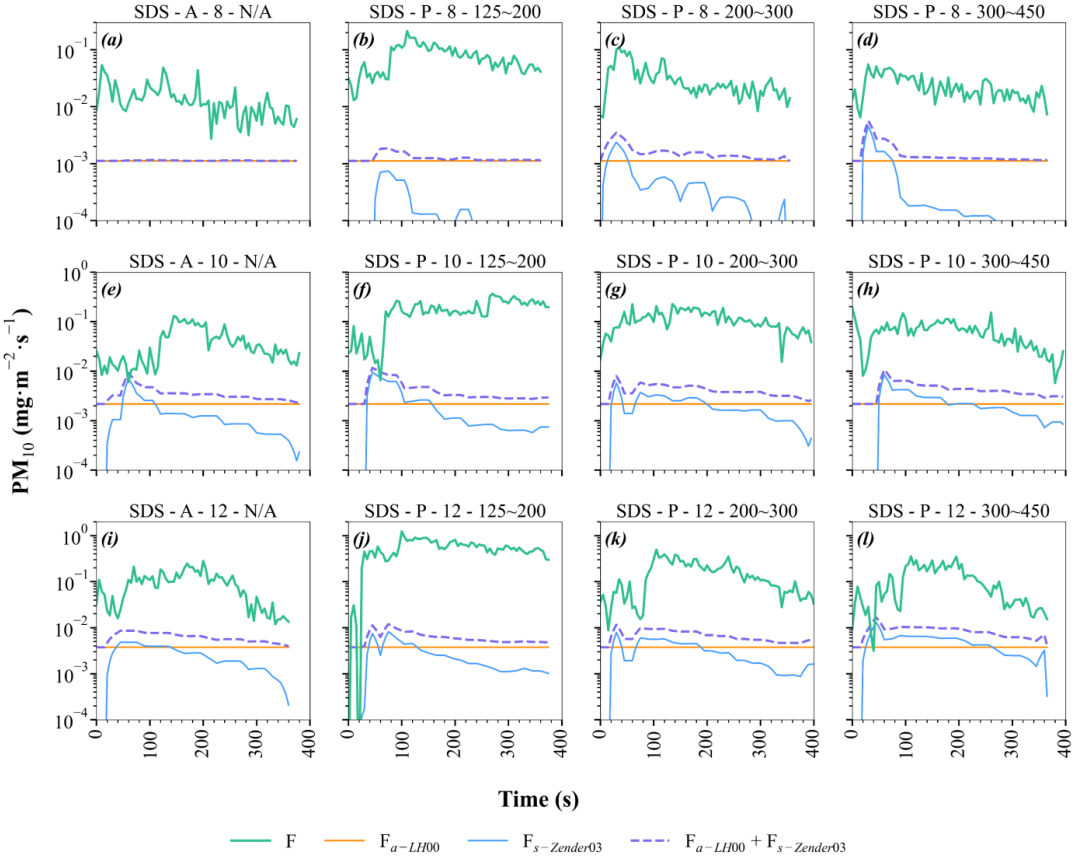

Figure 5. Time series variations in the mean values of *F*, $F_{a\text{-}LH00}$, $F_{s\text{-}zender03}$, and $F_{a\text{-}LH00} + F_{s\text{-}zender03}$ for the SDS-*x*-*y*-*z* experiments. Each panel shows data from the corresponding sub-experiment.

https://doi.org/10.5194/egusphere-2026-3563
Preprint. Discussion started: 8 July 2026
© Author(s) 2026. CC BY 4.0 License.

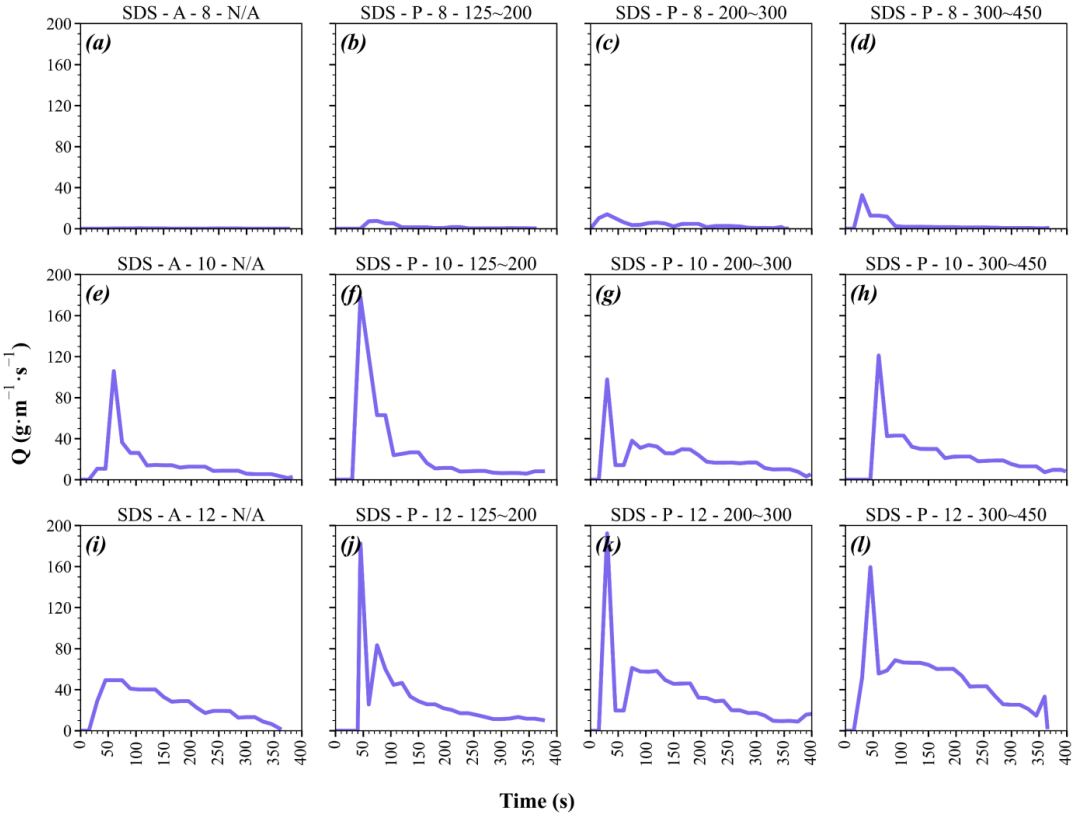

Figure 6. Time-series variations of *Q* in SDS-*x*-*y*-*z* experiments. Each panel shows data from the corresponding sub-experiment.

3.3.2 Quantitative contribution of aerodynamic entrainment to total PM_{10} emission

For the desert steppe experiment at a wind speed of 8 $m \cdot s^{-1}$ (SDS-x-8-z), the emission in the absence of sand supply (SDS-A-8-N/A) is exclusively driven by aerodynamic entrainment, yielding a cumulative emission of 5.35 $mg \cdot m^{-2}$ over the unified period (Figure 7a). Conservatively neglecting any potential enhancement of aerodynamic entrainment by saltation bombardment, this value can be regarded as the cumulative aerodynamic entrainment emission at this wind speed. Consequently, this cumulative amount accounted for 19.35%, 46.09%, and 62.43% of the total PM_{10} emissions in the corresponding sand-supplied experiments (SDS-P-8-125~200, SDS-P-8-200~300, and SDS-P-8-300~450, respectively). Such substantial proportions unequivocally demonstrate that the contribution of aerodynamic entrainment is highly significant and cannot be neglected under these wind conditions.

Furthermore, comparing the cumulative PM_{10} emissions across varying wind speeds within the no-sand-supply group (SDS-A-x-N/A) further quantifies the minimum contribution of aerodynamic entrainment. Adopting the cumulative emission from the SDS-A-8-N/A experiment (5.35 $mg \cdot m^{-2}$) as a conservative baseline for aerodynamic entrainment, this value accounts

https://doi.org/10.5194/egusphere-2026-3563
Preprint. Discussion started: 8 July 2026
© Author(s) 2026. CC BY 4.0 License.

for 35.76% and 16.09% of the total cumulative emissions in the SDS-A-10-N/A and SDS-A-12-N/A experiments, respectively. Given that the intensity of aerodynamic entrainment scales non-linearly with wind speed, the actual PM_{10} mass generated by direct entrainment at 10 $m \cdot s^{-1}$ and 12 $m \cdot s^{-1}$ must exceed this baseline. Consequently, the true proportional contributions of aerodynamic entrainment under these higher wind regimes are greater than 35.76% and 16.09%, respectively. These results confirm that as wind speed increases, aerodynamic entrainment consistently constitutes a substantial and non-negligible fraction of the total PM_{10} emission.

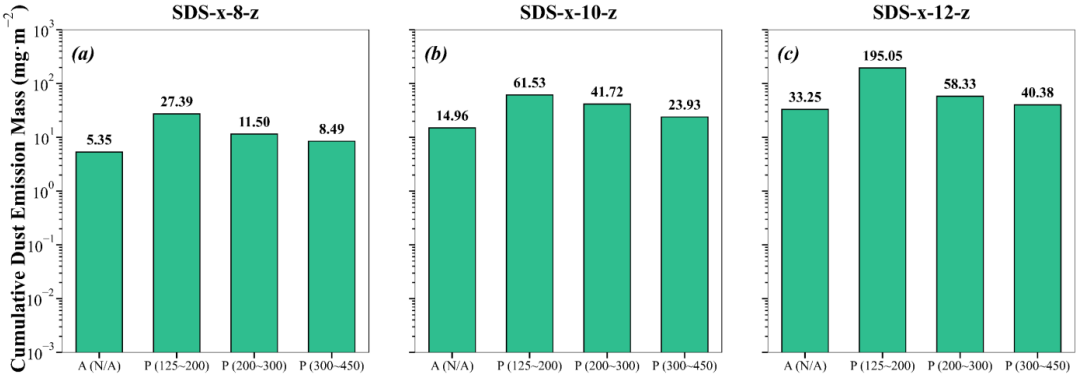

Figure 7. Cumulative emission of PM_{10} over the same emission period for each experiment.

3.3.3 Enhanced aerodynamic entrainment by saltation

Previous analyses have demonstrated that the *F* in SDS-A-8-N/A experiment originated almost entirely from aerodynamic entrainment. Subtracting the cumulative PM_{10} emission of SDS-A-8-N/A from those of SDS-P-08-200~300 and SDS-P-08-300~450 under the same wind speed yields differences of 6.15 and 3.14 $mg \cdot g^{-1}$, respectively (Figure 7). Even if the larger difference (6.15 $mg \cdot g^{-1}$) is conservatively assumed to represent the entire saltation-related emission contribution in SDS-P-08-125~200, the remaining aerodynamic entrainment emission is still 21.24 $mg \cdot g^{-1}$, nearly four times the 5.35 $mg \cdot g^{-1}$ observed in SDS-A-8-N/A. Since SDS-P-08-125~200 actually produced only 1/2.48 of the cumulative horizontal saltation flux of SDS-P-08-200~300, this assumption overestimates the saltation contribution. These results indicate that saltation bombardment substantially enhances aerodynamic entrainment.

On the other hand, at the wind speed of 8 m/s, the *Q* in SDS-P-08-125~200 was almost consistently lower than those in SDS-P-08-200~300 and SDS-P-08-300~450 (Figure 6). In terms of cumulative horizontal saltation flux, SDS-P-08-300~450 reached 1.41 $kg \cdot m^{-1}$, 2.43 times that of SDS-P-08-125~200, and SDS-P-08-200~300 reached 1.44 $kg \cdot m^{-1}$, 2.48 times that of SDS-P-08-125~200 (Figure 8a). However, the *F* in SDS-P-08-200~300 and SDS-P-08-300~450 remained consistently lower than that in SDS-P-08-125~200. Quantitatively, the cumulative PM_{10} emission of SDS-P-08-125~200 was 2.38 and 3.22 times that of SDS-P-08-200~300 and SDS-P-08-300~450, respectively. A similar phenomenon was observed at the wind speed of

https://doi.org/10.5194/egusphere-2026-3563
Preprint. Discussion started: 8 July 2026
© Author(s) 2026. CC BY 4.0 License.

12 m/s (Figure 6, Figure 8c). That is, the experiment with the finer saltating particles (SDS-P-08-125~200) emitted substantially more dust despite having a lower saltation flux. Classical bombardment theory holds that the dust emission flux generated by saltation bombardment is proportional to the horizontal saltation flux ($F=\alpha \cdot Q$), which is clearly contradicted by the above observation. This contradiction indicates that the total dust emission flux is not fully governed by the horizontal saltation flux. The finer saltating particles, with their higher number density, exerted stronger abrasion and fragmentation on the surface. We speculate that this bombardment disturbance may not only directly eject some of the loose surface dust and the dust produced by aggregate disintegration into the atmosphere, but also leave a fraction of the disintegration-generated dust on the surface, thereby enhancing and amplifying aerodynamic entrainment.

Further comparison of SDS-P-10-125~200 and SDS-P-12-125~200 shows that their cumulative horizontal saltation fluxes were nearly identical (9.65 and 9.94 $kg \cdot m^{-1}$, respectively), whereas cumulative PM_{10} emission differed by 133.52 $mg \cdot m^{-2}$. According to classical bombardment theory, when saltation fluxes are comparable, the dust emission directly produced by saltation bombardment should be roughly equal; the measured total emissions, however, differ markedly. This further indicates that saltation bombardment not only directly ejects some of the loose surface dust and the dust generated by aggregate disintegration into the atmosphere, but also leaves a portion of the disintegration-derived dust on the surface; this liberated dust is subsequently entrained into the atmosphere by the shear stress of the airflow. Moreover, when loose surface dust is abundant, the greater airflow shear stress would generate larger amount of dust deflation.

In most of the experiments, when Q increased abruptly, F generally did not respond to this change immediately but lagged behind (Figures 5 and 6). This finding further proved our speculation that saltation can act as a disturbance that changes the surface properties through bombardment and abrasion, which renews the surface and enriches the available finer particles. Therefore, the increasing dust emission flux derived from direct aerodynamic entrainment was triggered. In other words, the saltation disturbance enhanced the direct aerodynamic entrainment of dust.

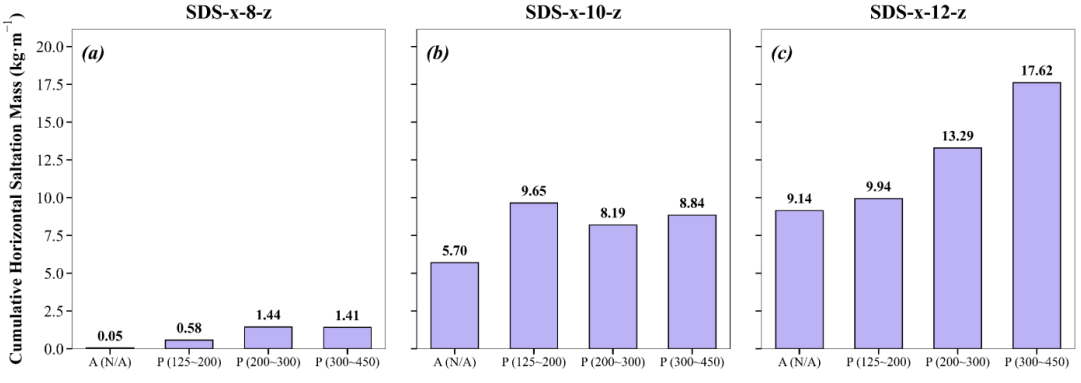

Figure 8. Cumulative horizontal saltation mass over the same emission period for each experiment

https://doi.org/10.5194/egusphere-2026-3563
Preprint. Discussion started: 8 July 2026
© Author(s) 2026. CC BY 4.0 License.

3.3.4 Dynamic nature of dust emission and limitations of existing models

In all the experiments under constant wind speeds, the dust emission rates experienced multiple fluctuations, and they usually had several peaks. After reaching a peak, the dust emission rate generally decreased rapidly, followed by periodic fluctuations (Figure 5). These findings suggest that the dust emission process is closely linked to the dynamic renewal of the surface. When dust emission reaches its peak, F decreases rapidly because the supply of readily erodible fine particles becomes temporarily depleted. As the surface continues to renew under the disturbances of saltation (e.g., the breaking of surface crusts and aggregates, or the exposure of finer subsurface particles), F increases again, forming a new emission peak. This cyclic pattern reveals that dust emission does not occur over a static bed surface but rather evolves in concert with dynamically changing surface conditions.

To evaluate the ability of existing dust emission models to reproduce these dynamics, the calculated $F_{a\text{-}LH00}$, $F_{s\text{-}Zender03}$, and their sum were compared with the observed time series of F (Figure 5). Neither $F_{a\text{-}LH00}$ nor $F_{s\text{-}Zender03}$, whether considered individually or combined, was able to reproduce either the magnitude of observed dust emissions or their temporal variability.

The fundamental reason for this discrepancy is that both models are based on static or highly simplified representations of the soil surface and therefore fail to capture the continuous evolution of surface properties during wind erosion. The LH00 model relies solely on friction velocity and an empirical coefficient, without explicitly representing the physical processes governing dust emission or accounting for changes in surface conditions. Under constant wind-speed conditions in the wind tunnel, friction velocity remains effectively constant when the Owen effect is neglected, resulting in a temporally invariant $F_{a\text{-}LH00}$ that cannot reproduce the observed emission dynamics. Similarly, the Zender03 model parameterizes dust emission efficiency exclusively as a function of clay content and assumes an unlimited and temporally invariant supply of erodible material. Moreover, it neglects direct aerodynamic entrainment. Consequently, it is also unable to capture either the observed emission magnitude or its temporal evolution.

The substantial discrepancy between observed F and the combined estimate $F_{a\text{-}LH00} + F_{s\text{-}Zender03}$ further indicates that total dust emission cannot be interpreted as a simple linear superposition of contributions from individual emission mechanisms. As surface properties evolve during erosion, the relative importance of different emission pathways is likely to change continuously, while interactions among mechanisms may further modify their individual contributions. Dust emission should therefore be viewed as a dynamic, nonlinear process governed by the co-evolution of surface conditions and multiple interacting emission mechanisms.

4 Discussion

4.1 Dynamics of dust supply on natural surface

https://doi.org/10.5194/egusphere-2026-3563
Preprint. Discussion started: 8 July 2026
© Author(s) 2026. CC BY 4.0 License.

The conventional viewpoint suggests that a limited dust supply is a critical constraint on the sustained occurrence of direct aerodynamic entrainment in dust emission processes (Kok et al., 2012; Shao, 2008). However, our study demonstrated that "limited dust supply" is transient rather than persistent.

The field observation results revealed that in eight plots, predominantly in Scenario II, the duration of direct aerodynamic dust entrainment exceeded 3.5 hours, and in some plots, direct aerodynamic entrainment was maintained continuously throughout the entire observation period (Figure 3). The surfaces with a "limited dust supply" could not continue this process.

The results of the soil particle size analysis revealed that TFVa was not significantly correlated with the PM_{10} content (Figure 4). This result indicates that the persistence of dust emission does not depend on an initial reservoir of fine particles. Therefore, "limited dust supply" is a temporary state rather than a permanent one and may not be a dominant limitation during sustained wind erosion events.

The pronounced oscillations in *F* observed under constant wind speed conditions in the wind tunnel experiments (Figures 5) further confirm the occurrence of surface renewal processes. At the initial stage of the experiment, loose surface particles were rapidly emitted, causing an emission peak of dust. As fine particles subsequently became depleted, *F* temporarily decreased. With continued wind erosion, the subsurface layer was gradually exposed, and available finer particles were exposed, leading to a subsequent increase in *F*. This cyclical fluctuation indicated that the available fine particles were not statically limited but dynamically regenerated. These findings highlight the limitations of dust emission models based on static erodible beds, underscoring the need to incorporate dynamic supply mechanisms to improve numerical modeling accuracy. The interaction between these processes establishes a positive feedback loop of "erosion–renewal–entrainment." This underscores the critical role of accurately representing the influence of wind erosion, especially saltation disturbance, on the dynamic supply of available fine particles in improving dust emission parameterizations.

4.2 Enhancing effects of saltation disturbance on dust emission

Traditional theories posit that the core mechanism of saltation bombardment lies in the transfer of kinetic energy: saltating particles impact the surface, imparting momentum to finer particles and enabling them to be emitted by overcoming cohesive forces (Bagnold, 1941; Rice et al., 1996; Shao, 2001; Shao et al., 1993).

However, this mechanism is unable to explain our observations: if only the role of momentum transfer were the dominant control, coarser saltating particles with higher impact energy would be expected to produce stronger enhancement of dust emission. In contrast, wind tunnel experiments showed that the 125~200 μm saltation flux exerted the most pronounced enhancement on dust emission, exceeding that of the 200~300 μm and 300~400 μm size classes. This discrepancy suggests that saltation bombardment affects dust emission not only through instantaneous momentum transfer but also through

https://doi.org/10.5194/egusphere-2026-3563
Preprint. Discussion started: 8 July 2026
© Author(s) 2026. CC BY 4.0 License.

modification of surface conditions and the availability of erodible material.

To explain this phenomenon, we propose the conceptual framework illustrated in Figure 9. Under low wind speed conditions, loose fine particles are directly entrained into the atmosphere by the shear stress of airflow (Figure 9a). When wind speed exceeds the TFVs, saltating particles (including sand grains and aggregates) impact the surface and affect dust emission through multiple coupled processes (Figure. 9bcd). First, saltation impacts transfer momentum to surface fine particles, directly ejecting them into the atmosphere (Figure 9b). Second, impacts by saltating particles can mechanically disrupt soil crusts, disintegrate surface aggregates (abrasive action) or even cause the saltating aggregates themselves to fragment (Figure 9cd). These processes liberate fine particles originally encapsulated within crusts or aggregates, with some being emitted into the atmosphere and some remaining free on the surface, thereby replenishing the pool of erodible material and directly enhancing subsequent aerodynamic entrainment. Third, saltation bombardment dynamically alters the surface structure through two key mechanisms: (1) the displacement of surface particles exposes the finer material beneath (localized exposure) and (2) sustained impacts progressively erode the surface layer, ultimately revealing subsurface fines (abrasive exposure). Together, these processes constitute a surface renewal mechanism, sustaining the supply of erodible fines and reinforcing the efficiency of direct entrainment over time (Figure 9efg).

Field observations of delayed dust emission types, as well as lagged PM_{10} flux responses observed in wind tunnel experiments (Figure 5), further support this mechanism. These findings indicate that fine particles, once exposed or disaggregated by bombardment, can be subsequently entrained by wind, acting as an additional source of dust emissions. This effect was particularly pronounced in the 125~200 μm particle-size class. Although individual particles possessed lower impact energy than coarser grains, their higher impact frequency substantially increased the availability of erodible material. Notably, the processes of localized and abrasive exposure constitute a cyclic pattern of surface renewal. The periodic fluctuations observed in PM_{10} fluxes during wind tunnel experiments offer compelling evidence for the persistence and efficacy of this feedback mechanism.

This mechanism challenges the conventional assumption of dust supply limitations and enriches the understanding of the saltation bombardment process. Therefore, parameterizing dust emission processes should fully account for these dynamic interactions, incorporating key parameters such as the rate of surface renewal and the replenishment of entrainable sources to more accurately represent dust emission under natural conditions.

https://doi.org/10.5194/egusphere-2026-3563
Preprint. Discussion started: 8 July 2026
© Author(s) 2026. CC BY 4.0 License.

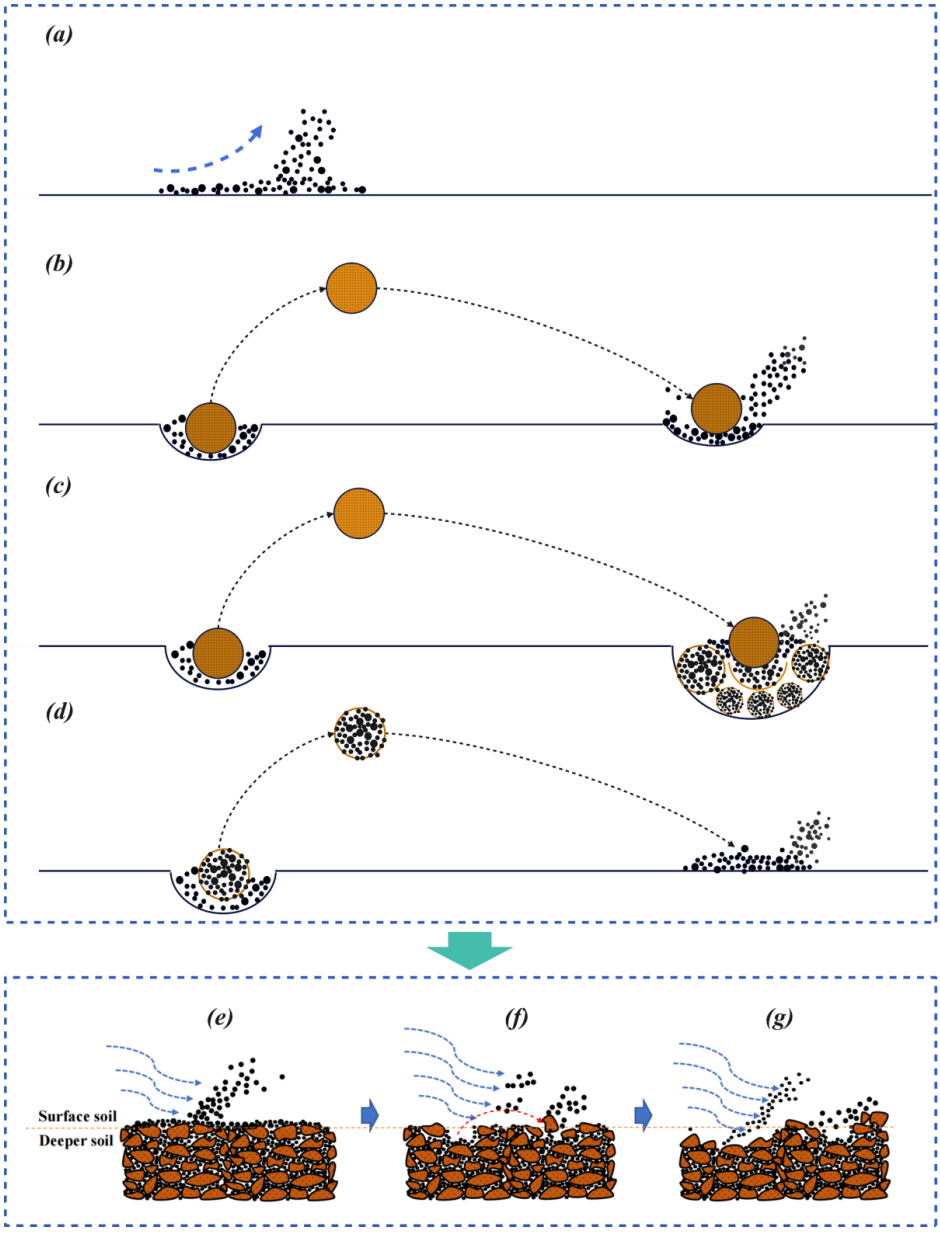

Figure 9. Conceptual diagram of dust emission mechanisms: (a) direct aerodynamic entrainment of fine particles from the surface; (b–d) saltation-induced processes, including (b) bombardment of the surface by saltating particles, enabling fine particles to overcome interparticle cohesion and be emitted into the atmosphere; (c) abrasion and disruption of soil crusts or aggregates by saltator impacts, leading to dust emission and exposure of subsurface fine particles; (d) fragmentation of saltating aggregates, resulting in dust emission and emission of free fine particles; (e–g) schematic representation of the complete dust emission process: (e) aerodynamic entrainment of surface fines; (f) saltation bombardment and associated emission; (g) surface disturbance exposing subsurface fine particles.

https://doi.org/10.5194/egusphere-2026-3563
Preprint. Discussion started: 8 July 2026
© Author(s) 2026. CC BY 4.0 License.

4.3 Implications for improving dust emission parameterization

This study revealed that significant discrepancies exist between the measured dust emission rates and the calculated rates derived from an empirical aerodynamic entrainment model and a traditional dust emission model that is based on a saltation bombardment mechanism (Figure 5). The empirical aerodynamic entrainment model does not account for specific physical processes and surface properties, and does not include dust emission caused by saltation; the traditional dust emission model based on a saltation bombardment mechanism neglects the process of direct aerodynamic entrainment, which is a major reason for the generation of uncertainty in dust emission simulations.

Based on the above new findings, the following important insights are provided for optimizing the dust emission model:

(1) Direct aerodynamic entrainment can occur continuously and can produce non-negligible amounts of emission, thus playing an important role in dust emissions. Consequently, the parameterization of dust emission processes should explicitly incorporate the direct aerodynamic entrainment mechanism.

(2) Beyond serving as vectors for kinetic energy transfer, saltating particles play a pivotal role in dust emission by inducing the fragmentation of surface crusts or soil aggregates through abrasion, and by continuously renewing the surface through abrasion and exposure processes—mechanisms that collectively increase the availability of erodible fine particles. Therefore, dust emission parameterizations should comprehensively account for the multiple roles of saltating particles.

(3) Dust emission exhibits a four-stage dynamic characteristic: “entrainment–saltation–renewal–entrainment”. At low wind speeds, loose fine particles at the surface are first directly entrained into the atmosphere. As the wind speed increases, sand grains or aggregates begin to saltate, with saltating particles transferring momentum to the surface via bombardment. This momentum overcomes the cohesive forces of fine particles, which emit them into the airstream. Simultaneously, the fragmentation of saltating aggregates not only directly causes the emission of some dust into the airflow, but also causes some fine dust to remain free on the surface; the impacts of saltating particles disrupt soil crusts or surface aggregates, causing dust emission while further generating fine particles that can be subsequently entrained by the airflow. The exposure effect of saltating particles and the abrasive effect enable the emission of underlying fine particles. These exposed fines are then entrained by the wind. Therefore, dust emission is the result of multiple interacting physical processes, with the surface evolving dynamically. Traditional models that rely solely on the linear extrapolation of saltation bombardment flux are inadequate for capturing the multiprocess synergy of natural dust emissions. Thus, a coupled “entrainment–saltation–renewal–entrainment” model that accounts for dynamic changes in the surface is necessary.

(4) Saltation bombardment not only facilitates the emission of fine particles by transferring momentum to the surface but also increases the quantity of fine particles available for direct entrainment, thereby playing a composite role in dust emission. Consequently, traditional methods that rely solely on the soil clay content to determine the bombardment efficiency of

https://doi.org/10.5194/egusphere-2026-3563
Preprint. Discussion started: 8 July 2026
© Author(s) 2026. CC BY 4.0 License.

dust emissions lack a scientific basis.

5. Conclusion

In this study, we integrate field observations with wind tunnel experiments to systematically investigate the persistence characteristics, contribution of aerodynamic entrainment to total dust emission, and role of saltation bombardment in dust emission.

Our results show that direct aerodynamic entrainment of dust can occur persistently in natural environments and produce non-negligible amounts of dust emission.

Saltation disturbance contributes to dust emission through three primary mechanisms: (1) the kinetic energy of saltating particles breaks the cohesive forces between fine particles, thereby emitting them into the airflow; (2) the disturbance causes fragmentation of saltating aggregates and breakage of soil crusts or surface aggregates (abrasive action), thereby causing dust emission and replenishing the pool of fine particles; and (3) through surface renewal by exposure and abrasion, the disturbance reveals subsurface fine particles. Moreover, saltation disturbances enhance the availability of entrainable fine particles through the latter two mechanisms, which in turn directly amplifies subsequent aerodynamic entrainment rather than through initial momentum transfer.

Dust emission manifests as a dynamic surface process involving a coupled set of mechanisms: “entrainment–saltation–renewal–entrainment”. Direct aerodynamic entrainment persists throughout the entire emission process and produces non-negligible dust flux. Conventional saltation bombardment models, which typically assume a static bed surface and neglect the role of direct entrainment, substantially underestimate total dust emissions. To more accurately capture the complex dynamics of dust emission under natural conditions, future models should incorporate direct aerodynamic entrainment process and embed it within a multimechanism coupled framework.

Data availability

The field observations and wind tunnel experimental data are available via the Figshare repository at *https://doi.org/10.6084/m9.figshare.30067912*

Author contributions

This paper was led by Shengfei Yang. Conceptualized by Shengfei Yang. Investigation by Shengfei Yang, Yawei Fan, Yongjie Liu. Methodology by Shengfei Yang, Yawei Fan. Software by Shengfei Yang. Resources by Heqiang Du, Zongxing

https://doi.org/10.5194/egusphere-2026-3563
Preprint. Discussion started: 8 July 2026
© Author(s) 2026. CC BY 4.0 License.

Li. Supervision by Heqiang Du, Zongxing Li. Project administration by Heqiang Du. Visualization by Shengfei Yang, Yawei Fan. Writing (original draft) by Shengfei Yang, Heqiang Du. All authors contributed to the validation, review, and editing of the work.

Competing interests

The contact author has declared that none of the authors has any competing interests.

Disclaimer

Copernicus Publications remains neutral with regard to jurisdictional claims made in the text, published maps, institutional affiliations, or any other geographical representation in this paper. While Copernicus Publications makes every effort to include appropriate place names, the final responsibility lies with the authors. Views expressed in the text are those of the authors and do not necessarily reflect the views of the publisher.

Acknowledgements

Wind tunnel experiments were carried out at the Gansu Desert Control Research Institute.

Financial support

This work was financially supported by the National Natural Science Foundation of China (No.42271016).

https://doi.org/10.5194/egusphere-2026-3563
Preprint. Discussion started: 8 July 2026
© Author(s) 2026. CC BY 4.0 License.

References

Anderson, R. and Haff, P.: Simulation of Eolian Saltation, Science (New York, N.Y.), 241, 820–3, https://doi.org/10.1126/science.241.4867.820, 1988.

Bagnold, R. A.: The Physics of Blown Sand and Desert Dunes, Springer Netherlands, Dordrecht, https://doi.org/10.1007/978-94-009-5682-7, 1941.

Du, H., Liu, X. L., Ding, R., Fan, Y., and Liu, X. F.: New insights into dust emission mechanism in natural environments based on a series of field observations, Science of The Total Environment, 914, 169888, https://doi.org/10.1016/j.scitotenv.2024.169888, 2024.

Dupont, S.: On the Influence of Thermal Stratification on Emitted Dust Flux, JGR Atmospheres, 127, e2022JD037364, https://doi.org/10.1029/2022JD037364, 2022.

Engelstaedter, S., Tegen, I., and Washington, R.: North African dust emissions and transport, Earth-Science Reviews, 79, 73–100, https://doi.org/10.1016/j.earscirev.2006.06.004, 2006.

Hansen, J., Sato, M., and Ruedy, R.: Radiative forcing and climate response, Journal of Geophysical Research: Atmospheres, 102, 6831–6864, https://doi.org/10.1029/96JD03436, 1997.

Haustein, K., Washington, R., King, J., Wiggs, G., Thomas, D. S. G., Eckardt, F. D., Bryant, R. G., and Menut, L.: Testing the performance of state-of-the-art dust emission schemes using DO4Models field data, Geoscientific Model Development, 8, 341–362, https://doi.org/10.5194/gmd-8-341-2015, 2015.

Huang, J., Lin, B., Minnis, P., Wang, T., Wang, X., Hu, Y., Yi, H., and Ayers, J.: Satellite-based assessment of possible dust aerosols semi-direct effect on cloud water path over East Asia, Geophysical Research Letters - GEOPHYS RES LETT, 33, https://doi.org/10.1029/2006GL026561, 2006.

Kjelgaard, J. F., Chandler, D. G., and Saxton, K. E.: Evidence for direct suspension of loessial soils on the Columbia Plateau, Earth Surface Processes and Landforms, 29, 221–236, https://doi.org/10.1002/esp.1028, 2004.

Klose, M. and Shao, Y.: Stochastic parameterization of dust emission and application to convective atmospheric conditions, Atmos. Chem. Phys., 12, 7309–7320, https://doi.org/10.5194/acp-12-7309-2012, 2012.

Klose, M., Shao, Y., Li, X., Zhang, H., Ishizuka, M., Mikami, M., and Leys, J. F.: Further development of a parameterization for convective turbulent dust emission and evaluation based on field observations, JGR Atmospheres, 119, 10441–10457, https://doi.org/10.1002/2014JD021688, 2014.

Kok, J. F., Parteli, E. J. R., Michaels, T. I., and Karam, D. B.: The physics of wind-blown sand and dust, Rep. Prog. Phys., 75, 106901, https://doi.org/10.1088/0034-4885/75/10/106901, 2012.

Koren, I., Kaufman, Y., Remer, L., and Martins, V.: Measurement of the Effect of Amazon Smoke on Inhibition of Cloud Formation, Science (New York, N.Y.), 303, 1342–5, https://doi.org/10.1126/science.1089424, 2004.

Li, J., Jian, B., Huang, J., Hu, Y., Zhao, C., Kawamoto, K., Shujie, L., and Wu, M.: Long-term variation of cloud droplet number concentrations from space- based Lidar, Remote Sensing of Environment, 213, https://doi.org/10.1016/j.rse.2018.05.011, 2018.

Liao, H. and Seinfeld, J.: Radiative forcing by mineral dust aerosols: Sensitivity to key variables, Journal of Geophysical

https://doi.org/10.5194/egusphere-2026-3563
Preprint. Discussion started: 8 July 2026
© Author(s) 2026. CC BY 4.0 License.

Research, 1033, 31637–31646, https://doi.org/10.1029/1998JD200036, 1998.

Liu, J., Han, Y., Tang, X., Zhu, J., and Zhu, T.: Estimating adult mortality attributable to PM2.5 exposure in China with assimilated PM2.5 concentrations based on a ground monitoring network, Science of The Total Environment, 568, 1253–1262, https://doi.org/10.1016/j.scitotenv.2016.05.165, 2016.

Loosmore, G. A. and Hunt, J. R.: Dust resuspension without saltation, Journal of Geophysical Research: Atmospheres, 105, 20663–20671, https://doi.org/10.1029/2000JD900271, 2000.

Macpherson, T., Nickling, W. G., Gillies, J. A., and Etyemezian, V.: Dust emissions from undisturbed and disturbed supply-limited desert surfaces, Journal of Geophysical Research: Earth Surface, 113, https://doi.org/10.1029/2007JF000800, 2008.

Marticorena, B. and Bergametti, G.: Modeling the atmospheric dust cycle: 1. Design of a soil-derived dust emission scheme, Journal of Geophysical Research: Atmospheres, 100, 16415–16430, https://doi.org/10.1029/95JD00690, 1995.

Ravi, S., D'Odorico, P., Breshears, D., Field, J., Goudie, A., Huxman, T., Li, J., Okin, G., Swap, R., Thomas, A., Van Pelt, R., and Whicker, J.: Aeolian processes and the biosphere, Reviews of Geophysics, 49, https://doi.org/10.1029/2010RG000328, 2011.

Rice, M. A., Willetts, B. B., and McEWAN, I. K.: Wind Erosion of Crusted Soil Sediments, Earth Surface Processes and Landforms, 21, 279–293, https://doi.org/10.1002/(SICI)1096-9837(199603)21:3%3C279::AID-ESP633%3E3.0.CO;2-A, 1996.

Ridgwell, A. J. and Watson, A. J.: Feedback between aeolian dust, climate, and atmospheric CO2 in glacial time, Paleoceanography, 17, 11-1-11–11, https://doi.org/10.1029/2001PA000729, 2002.

Shao, Y.: A model for mineral dust emission, Journal of Geophysical Research: Atmospheres, 106, 20239–20254, https://doi.org/10.1029/2001JD900171, 2001.

Shao, Y. (Ed.): Physics and Modelling of Wind Erosion, in: Physics and Modelling of Wind Erosion, Springer Netherlands, Dordrecht, 303–360, https://doi.org/10.1007/978-1-4020-8895-7_9, 2008.

Shao, Y. and Dong, C. H.: A review on East Asian dust storm climate, modelling and monitoring, Global and Planetary Change, 52, 1–22, https://doi.org/10.1016/j.gloplacha.2006.02.011, 2006.

Shao, Y. and Klose, M.: A note on the stochastic nature of particle cohesive force and implications to threshold friction velocity for aerodynamic dust entrainment, Aeolian Research, 22, 123–125, https://doi.org/10.1016/j.aeolia.2016.08.004, 2016.

Shao, Y. and Raupach, M. R.: The overshoot and equilibration of saltation, Journal of Geophysical Research: Atmospheres, 97, 20559–20564, https://doi.org/10.1029/92JD02011, 1992.

Shao, Y., Raupach, M., and Findlater, P.: Effect of Saltation Bombardment on the Entrainment of Dust by Wind, Journal of Geophysical Research, 98, 12719–12726, https://doi.org/10.1029/93JD00396, 1993.

Shao, Y., Chen, S., Huang, N., Gui, H., Mao, R., Masahide, I., Wu, C., Yin, X., and Zhang, J.: Source Limitation Could Have Major Implications to Dust Emission Estimates, Geophysical Research Letters, 52, e2024GL112562, https://doi.org/10.1029/2024GL112562, 2025.

https://doi.org/10.5194/egusphere-2026-3563
Preprint. Discussion started: 8 July 2026
© Author(s) 2026. CC BY 4.0 License.

Sharratt, B., Feng, G., and Wendling, L.: Loss of soil and PM10 from agricultural fields associated with high winds on the Columbia Plateau, Earth Surf Processes Landf, 32, 621–630, https://doi.org/10.1002/esp.1425, 2007.

Sokolik, I. N. and Toon, O. B.: Incorporation of mineralogical composition into models of the radiative properties of mineral aerosol from UV to IR wavelengths, Journal of Geophysical Research: Atmospheres, 104, 9423–9444, https://doi.org/10.1029/1998JD200048, 1999.

Sweeney, M. R. and Mason, J. A.: Mechanisms of dust emission from Pleistocene loess deposits, Nebraska, USA, Journal of Geophysical Research: Earth Surface, 118, 1460–1471, https://doi.org/10.1002/jgrf.20101, 2013.

Thompson, J. M. T. and Ridgwell, A. J.: Dust in the Earth system: the biogeochemical linking of land, air and sea, Philosophical Transactions of the Royal Society of London. Series A: Mathematical, Physical and Engineering Sciences, 360, 2905–2924, https://doi.org/10.1098/rsta.2002.1096, 2002.

Újvári, G., Kok, J., Varga, G., and Kovács, J.: The physics of wind-blown loess: Implications for grain size proxy interpretations in Quaternary paleoclimate studies, Earth-Science Reviews, 154, https://doi.org/10.1016/j.earscirev.2016.01.006, 2016.

Wagner, R., Schepanski, K., and Klose, M.: The Dust Emission Potential of Agricultural-Like Fires—Theoretical Estimates From Two Conceptually Different Dust Emission Parameterizations, JGR Atmospheres, 126, e2020JD034355, https://doi.org/10.1029/2020JD034355, 2021.

Zakey, A. S., Solmon, F., and Giorgi, F.: Implementation and testing of a desert dust module in a regional climate model, Atmospheric Chemistry and Physics, 6, 4687–4704, https://doi.org/10.5194/acp-6-4687-2006, 2006.

Zender, C. S., Bian, H., and Newman, D.: Mineral Dust Entrainment and Deposition (DEAD) model: Description and 1990s dust climatology, Journal of Geophysical Research: Atmospheres, 108, https://doi.org/10.1029/2002JD002775, 2003.

Zhang, J., Teng, Z., Huang, N., Guo, L., and Shao, Y.: Surface Renewal as a Significant Mechanism for Dust Emission, Atmospheric Chemistry and Physics Discussions, 1–22, https://doi.org/10.5194/acp-2016-421, 2016.

Zhang, J., Li, G., Shi, L., Huang, N., and Shao, Y.: Impact of turbulence on aeolian particle entrainment: results from wind-tunnel experiments, Atmos. Chem. Phys., 22, 9525–9535, https://doi.org/10.5194/acp-22-9525-2022, 2022.

Zhao, J., Ma, X., Wu, S., and Sha, T.: Dust emission and transport in Northwest China: WRF-Chem simulation and comparisons with multi-sensor observations, Atmospheric Research, 241, 104978, https://doi.org/10.1016/j.atmosres.2020.104978, 2020.

Zhu, Q., Liu, Y., Shao, T., and Tang, Y.: Transport of Asian aerosols to the Pacific Ocean, Atmospheric Research, 234, 104735, https://doi.org/10.1016/j.atmosres.2019.104735, 2019.